Toward Models for the Full Oxygen-Evolving Complex of Photosystem II by Ligand Coordination to Lower the Symmetry of the Mn_3CaO_4 Cubane: Demonstration that Electronic Effects Facilitate Binding of a Fifth Metal

Jacob S. Kanady, Po-Heng Lin, Kurtis M. Carsch, Robert J. Nielsen, Michael K. Takase, William A. Goddard III, and Theodor Agapie*

Divison of Chemistry and Chemical Engineering, California Institute of Technology, Pasadena, California 91125, United States

Supporting Online Material

Contents

General Considerations

Reactions performed under inert atmosphere were carried out in a glovebox or using standard Schlenk techniques under a nitrogen atmosphere. Solvents for air- and moisture-sensitive reactions were dried over sodium benzophenone ketyl, calcium hydride, or by the method of Grubbs.[1] Deuterated solvents were purchased from Cambridge Isotope Laboratories and vacuum transferred from sodium benzophenone ketyl (C_6D_6), calcium hydride (CD_2Cl_2) or used as received (DMSO-d_6). All solvents, once dried and degassed, were stored under inert atmosphere over 4 Å molecular sieves. Anhydrous *N,N*-dimethylformamide (DMF) was purchased from Aldrich and stored over molecular sieves. ^{1}H and ^{19}F NMR spectra were recorded on a Varian 300 MHz instrument at room temperature, and $^{13}C\{^{1}H\}$ NMR spectra were recorded on a Varian INOVA-500 MHz spectrometer at room temperature. Shifts are reported relative to the residual solvent peak. For paramagnetic samples, the window was –100 to 100 ppm, the acquisition time was 300 ms, the relaxation delay was set to 0 s, and ≥ 320 scans were taken on samples ≤5 mM in concentration to get good signal-to-noise. Robertson Microlit Laboratories, Ledgewood, NJ, performed elemental analyses. Electrospray Ionization Mass Spectrometry and high resolution MS were performed in the positive ion mode using an LCQ ion trap mass spectrometer (Thermo) at the California Institute of Technology Mass Spectra Facility.

2-[*N,N*-Bis(trimethylsilyloxy)]aminopropene was synthesized following a literature procedure.[2] In our hands, slow addition of the reaction mixture into the cold $NaHSO_4$ solution during work up was crucial in keeping the product from decomposing. *N,N′*-dimethylethylenediamine was distilled from KOH at atmospheric pressure, then distilled from Na^0. $LMn_3(OAc)_3$,[3] $Mn(OTf)_2{\bullet}CH_3CN$,[4] LutHOTf,[5] and $[LMn^{IV}_3GdO_4(OAc)_3(DMF)_2]OTf$ (**3**)[6] were synthesized as recently reported.

Synthetic Procedures

***N,N′*-dimethyl-*N,N′*-bis(propanone-oxime)-ethylenediamine (HON_4OH):** Following the work of Ioffe *et al.*,[7] 2-[*N,N*-bis(trimethylsilyloxy)]aminopropene (75 wt% with pentane, 7.29 g, 23.42 mmol, 2.2 equiv) was added to an oven-dried 100 mL round bottom with a stirbar sealed with a septum under N_2 by syringe and needle. *N,N′*-dimethylethylenediamine (0.94 g, 10.6 mmol) was transferred to oven-dried 25 mL round bottom sealed with a septum under N_2 by syringe and needle. Both compounds were diluted with dry dichloromethane (23 mL & 10.6 mL, respectively, 1 M each). The diamine solution was then cannula transferred to the bis(trimethylsilyloxy)]aminopropene

solution. Dichloromethane (3 mL) was used to rinse the 25 mL round bottom and cannula. The homogeneous yellow solution was stirred at room temperature for 8 hours, at which point the reaction mixture was poured into MeOH (*ca.* 250 mL). This yellow solution sat unstirred for 6 hours, at which point volatiles were removed *in vacuo* to give an orange oil. Trituration in hexane caused the oil to solidify, and after decanting the hexane, trituration in Et_2O and decanting again, an orange powder produced. The orange powder was then triturated in CH_3CN, giving an orange solution and white powder that was collected on a medium frit. The powder was rinsed with CH_3CN until all color was lost from the powder, which was then dried *in vacuo* for 8 hours (1.7 g, 69.6%). To further dry, the powder was rinsed on a frit with dry CH_3CN in the glovebox and any remaining CH_3CN was removed *in vacuo* (1.6 g , 65.5%).^{1}H NMR (300 MHz, DMSO-d_6, 25 °C): δ 10.47 (s, 2H, NO*H*), 2.90 (s, 4H, N–C*H*$_2$–C=N) , 2.38 (s, 4H, N–C*H*$_2$–), 2.07 (s, 6H, *H*$_3$C–N), 1.72 (s, 6H, *H*$_3$C–C=NOH). ^{13}C{^{1}H} NMR (126 MHz, DMSO-d_6, 25 °C): δ 154.66 (*C*=NOH), 61.95 (N–*CH*$_2$–C=N), 55.11 (N–*CH*$_2$), 42.60 (*H*$_3$*C*–N), 12.57 (*H*$_3$*C*–C=NOH). HRMS (FAB+): calcd. for $C_{10}H_{23}N_4O_2$ [M+H]: 231.1821; found: 231.1826.

$LMn^{IV}_3CaO_4(OAc)_3$•THF (1): Improving upon literature procedures,[3, 8] $LMn_3(OAc)_3$ (10.89 g, 8.6 mmol) and $Ca(OTf)_2$ (3.05 g, 9.0 mmol, 1.05 equiv) were mixed as solids in a 2 L round bottom flask with a stir bar inside a glovebox. THF (*ca.* 830 mL) and DME (*ca.* 70 mL) were added and the solution was stirred for 15-20 minutes before well-powdered KO_2 (1.83 g, 25.7 mmol, 3 equiv) was added slowly over 5-10 minutes. THF (*ca.* 30 mL) and DME (*ca.* 16 mL) were added to rinse down any KO_2 on the walls and to bring the final concentration to 9 mM and a ratio of 10:1 THF/DME. The round bottom was sealed with a 180º joint, taken out of the glovebox, and magnetically stirred. The solution changed colors from tan at 20 minutes, to brown at 45 minutes, grey-purple at 2 hours, and dark brown at 20 hours. At four days, red, crystalline precipitate was observed, and by seven days the solution also had a reddish hue. On the eighth day, the pressure was reduced inside the flask to more safely bring it back into the glovebox, where the red crystalline precipitate was collected by filtration of the reaction mixture through a celite pad on a 150 mL fritted funnel. The solid was rinsed with 100-150 mL CH_3CN (until no color is visible in the CH_3CN). The remaining solid was scraped into a 500 mL round bottom flask, residual CH_3CN was removed *in vacuo*, and the solid was triturated in a mixture of THF (150 mL) and benzene (20 mL) for *ca.* 20 minutes. The resulting mixture was filtered through a pad of celite, giving a red solution and red solid, which was scraped back into the 500 mL flask and re-triturated in THF/C_6H_6 to extract more product. This process of trituration and filtration was repeated until little to no color was observed in the filtered solution (*ca.* 3 x 200 mL THF/C_6H_6). The remaining solid was triturated in DMF (*ca.* 80 mL) and filtered to give a red solution separate from the THF/C_6H_6 fraction. At this point three solutions exist: the THF/DME/CH_3CN solution from filtration of the reaction mixture, the THF/C_6H_6 fraction, and the DMF fraction. All were taken out of the glovebox and volatiles were removed by vacuum distillation. The red residue from the THF/C_6H_6 fraction is pure **1** (2.3 g, 20% yield), while the red residue from the DMF fraction (0.7 g, 6%) may contain some potassium salts. The residue from the THF/DME/CH_3CN fraction was brought back into the glovebox, triturated in CH_3CN, and collected on a pad of celite. The solid was rinsed with CH_3CN until no more color came through, and then proceeded with the THF/C_6H_6 trituration and filtration cycle

performed above. The red solution was concentrated *in vacuo* to give more red powder **1** (1 g, 9%). The total yield was approximately 35%. Spectroscopic and electrochemical features match the literature,[8] although herein we report the ^{1}H NMR and UV-Vis spectroscopic features for the first time: ^{1}H NMR (300 MHz, C_6D_6 with a drop of THF for solubility, 25 ºC): 21.4, 11.3, 10.0, 8.6, 5.9, 5.1, -16.9 ppm. UV-Vis (λ_{max} (nm) [ε (M^{-1} cm^{-1})]): 245 ($8.0x10^4$), 310 ($2.2x10^4$), 365 ($1.1x10^4$), 490 ($2.0x10^3$), 710 ($3.5x10^2$).

$LMn^{III}_2Mn^{IV}_2O_4(OAc)_3$ (2) from $LMn^{IV}_3CaO_4(OAc)_3$•THF (1): Complex **1** (6.8 mg, 5 μmol) was dissolved in DMF (*ca.* 1.5 mL) to give a red/brown, homogeneous solution. Separately dissolved $Mn(OTf)_2$•CH_3CN (2.0 mg, 5 μmol) in DMF (*ca.* 0.5 mL) to give a clear and colorless solution, which was then added to the solution of **1**. The solution turns from red/brown to brown within 30 seconds of addition. The solution was allowed to stir ca. 30 minutes, then removed volatiles *in vacuo*. The resulting brown residue was extracted with benzene, which was filtered and concentrated to dryness to afford **2** (6.5 mg, *ca.* 100%). Spectral features match those found in previous work.[3, 8]

$[LMn^{IV}_3GdO_4(ON_4O)(OAc)(DMF)]OTf$ (4): In the glove box, a solution of **HON_4OH** (2.6 mg, 0.01 mmol, 1 equiv) and Et_3N (0.02 mmole, 2 equiv) in THF (2 mL) was added to $[LMn_3GdO_4(OAc)_3](OTf)$ (**3**) (15.6 mg, 0.01 mmol) in THF (2 mL). The dark brown solution was stirred magnetically for 12 hours and the solution was concentrated *in vacuo* to afford a brown solid. Crystals were obtained from DMF/THF/diethyl ether to yield the product as dark-brown crystals (15 mg, 91%). The NMR spectra were obtained in CD_2Cl_2 and then concentrated to dryness for elemental analysis. ^{1}H NMR (CD_2Cl_2, 300 MHz, 25ºC): δ 18.6, 11.7, 10.9, 10.3, 9.4, 9.0, 8.7, 6.8, 4.4, -17.4 ppm. ^{19}F NMR (CD_2Cl_2, 282 MHz, 25 ºC): δ -78.2 ppm. Anal. Calcd. For $C_{76}H_{75}Cl_6F_3GdMn_3N_{11}O_{15}S$ (**4**•$3CH_2Cl_2$): C, 45.50; H, 3.77; N, 7.68. Found: C, 45.68; H, 3.44; N, 8.11. UV-Vis (λ_{max} [ε (M^{-1} cm^{-1})]): 246 ($9.6x10^4$), 310 ($2.6x10^4$), 550 ($1.5x10^3$), 710 ($1.5x10^2$) nm.

$LMn^{IV}_3CaO_4(ON_4O)(OAc)$ (5): In a N_2 glovebox, an oven-dried Schlenk tube with stirbar was charged with **1** (301 mg, 0.22 mmol) and dry DMF (50 mL). **HON_4OH** (53 mg, 0.23 mmol, 1.05 equiv) was separately dissolved in dry DMF (5 mL) and the resulting clear and colorless solution was added to the red/brown and clear solution of **1**. The Schlenk tube was sealed, brought out of the glovebox and heated to 80 ºC in an oil bath for 40 minutes during which precipitate appeared in the solution. The volatiles were removed *in vacuo*. Back inside the glovebox, the red/brown residue was suspended in dry CH_3CN and volatiles were removed *in vacuo* again to remove any remaining DMF. After further trituration with CH_3CN (15-20 mL), the solids were collected on Celite and rinsed with CH_3CN until it ran colorless. The solids, along with some Celite from the filtration, were triturated in CH_2Cl_2 to extract the product and filtered through Celite. Any undissolved solid was re-triturated until the CH_2Cl_2 runs colorless (*ca.* 3 cycles or 10-30 mL). Removed volatiles *in vacuo* to afford red/brown **3** as a powder (130 mg, 42%). ^{1}H NMR (300 MHz, CD_2Cl_2, 25 ºC) 59.9, 22.6, 11.4, 10.8, 10.3, 8.6, 8.5, 8.1, 8.0, 7.0, 6.8, 4.9, 4.7, -13.2 ppm. Anal. Calcd. for $C_{75.5}H_{78}N_{10}O_{12.5}Mn_3CaCl$ (**5**•$1.5E_2O$•$0.5CH_2Cl_2$: C, 57.91; H, 5.02; N, 8.95. Found: C, 57.73; H, 4.78; N, 8.69. ***5** was triturated in Et_2O and concentrated to dryness three times in an attempt to remove the CH_2Cl_2. UV-Vis (λ_{max} (nm) [ε (M^{-1} cm^{-1})]): 240 ($7.3x10^4$), 315 ($1.8x10^4$), 500 ($1.8x10^3$), 705 ($7.0x10^1$).

[LMn$^{IV}_3$CaO$_3$(OH)(ON$_4$O)(OAc)]OTf (6): In the glovebox, to partially dissolved **3** (30.4 mg, 0.022 mmol) in CH_2Cl_2 (*ca.* 9 mL) was added dropwise LutHOTf (5.8 mg, 0.023 mmol, 1.05 equiv) as a clear and colorless solution in CH_2Cl_2 (*ca.* 2 mL). As the LutHOTf is added to the stirred solution of **3**, the solution becomes red/brown and heterogenous to darker red/brown and homogeneous. The LutHOTf vial was rinsed three times to ensure the full equivalent was added (total reaction volume is *ca.* 13 mL). The solution was filtered after 3 hours and removed volatiles *in vacuo*. The resulting red/brown solid was extracted with hexane followed by Et_2O to remove the resulting lutidine. The remaining material was extracted into C_6H_6, filtered through Celite, and concentrated to dryness to afford red/brown solid **6** (34 mg, *ca.* 100%). Crystals amenable to XRD analysis were grown from vapor diffusion of Et_2O into a C_6H_6 solution of **6**. ^{1}H NMR (300 MHz, CD_2Cl_2, 25 ºC) 59.7, 51.3, 34.9, 22.5, 16.9, 11.3, 10.4, 10.0, 8.8, 6.8, -4.4, -8.4, -13.2, -18.3 ppm . ^{19}F NMR (282 MHz, CD_2Cl_2, 25 ºC): -76.5 ppm. UV-Vis (λ_{max} [ε (M^{-1} cm^{-1})]): 307 ($2.4x10^4$) nm. Anal. Calcd. for $C_{70}H_{63}CaF_3Mn_3N_{10}O_{14}S$: C, 53.82; H, 4.06; N, 8.97. Found: C, 53.57; H, 4.31; N, 8.65.

LMn$^{IV}_3$CaO$_4$(ON$_4$O)(OAc)•Ag(OTf) (7): In the glovebox, **5** (13.0 mg, 9 μmol) was partially dissolved in CH_2Cl_2 (ca. 12 mL). AgOTf (2.6 mg, 10 μmol, 1.1 equiv) was dissolved in CH_3CN (ca. 0.3 mL) and diluted with CH_2Cl_2 (*ca.* 1 mL). The clear and colorless AgOTf solution to the red/brown and heterogeneous solution of **5** dropwise. Within 5 minutes, the reaction mixture was clear and orange. At 11 hours the mixture was concentrated *in vacuo*. **5** was visible by ^{1}H NMR spectroscopy; therefore, excess AgOTf (1 mg, 4 μmol, *ca.* 0.4 equiv) was added as a solution in CH_3CN/CH_2Cl_2 and the resulting mixture was stirred for 15 hours and concentrated *in vacuo* to afford **7** as a red/brown solid. Crystals amenable to XRD analysis were grown from vapor diffusion of Et_2O into a CH_2Cl_2 solution of **7**. Upon repeating the procedure, 1.5-2.0 equivalents of AgOTf were found to be necessary to push the reaction to completion. ^{1}H NMR (300 MHz, CD_2Cl_2, 25 ºC) 46.1, 29.5, 26.9, 20.3, 14.0, 13.3, 11.2, 8.8, 8.5, 7.9, 6.7, 5.9, 4.0, -5.3, -9.1, -12.7 ppm. ^{19}F NMR (282 MHz, CD_2Cl_2, 25 ºC): -76.5 ppm Anal. Calcd. for $C_{72}H_{64}Ag_2CaCl_2F_6Mn_3N_{10}O_{17}S_2$ (**7**•AgOTf•CH_2Cl_2): C, 43.00; H, 3.21; N, 6.97. Found: C, 43.32; H, 3.05; N, 6.96. *The excess AgOTf necessary to push the reaction to completion precipitated alongside **7** upon vapor diffusion of Et_2O into the CH_2Cl_2 solution of **7** and was difficult to remove by washing, as polar solvents that would extract AgOTf decompose **7**. These were therefore analyzed together, giving the extra equivalent of AgOTf in the analysis. **7** is known to crystallize with solvents in the lattice, so a CH_2Cl_2 molecule is also observed. UV-Vis (λ_{max} [ε (M^{-1} cm^{-1})]): 240 ($7.1x10^4$), 310 ($2.0x10^4$), 710 ($1.5x10^2$) nm.

Reaction of LMn$^{IV}_3$CaO$_4$(OAc)$_3$•THF (1) with LutHOTf: In the glovebox, **1** (13.9 mg, 0.01 mmol) was partially dissolved in CH_2Cl_2 (4 mL) to give a red/brown, heterogeneous mixture. A solution of LutHOTf (2.7 mg, 0.01 mmol, 1.05 equiv) in CH_2Cl_2 (1 ml) was added, and the LutHOTf vial was rinsed three times to ensure the full equivalent was added (total reaction volume is *ca.* 6 mL). The solution was stirred 6 hours, and did not homogenize like the reaction of **5** with LutHOTf. Volatiles were removed *in vacuo*, and

the residue was extracted with CH_2Cl_2, which contained LutHOTf (Figure S9, bottom), and then C_6D_6 with a drop of THF (Figure S9, top), which contained pure, unreacted **1**.

Reaction of $LMn^{IV}_3CaO_4(ON_4O)(OAc)$ (5) with $M(OTf)_2$ ($M=Mn^{2+}$, Co^{2+}): In the glovebox, **5** (14 mg, 0.01 mmol) was partially dissolved in CH_2Cl_2 (ca. 10 mL). $M(OTf)_2$ (0.013 mmol, 1.3 equiv) was dissolved in CH_3CN (ca. 0.5 mL) and diluted with CH_2Cl_2 (ca. 1 mL). The clear and colorless ($M=Mn^{2+}$) or clear and pink ($M=Co^{2+}$) solution was added dropwise to the red/brown and heterogeneous solution of **5**. Within 10 minutes the reaction mixture is clear. ESI-MS samples were prepared by diluting a small aliquot of the reaction mixture in CH_2Cl_2.

NMR Spectra

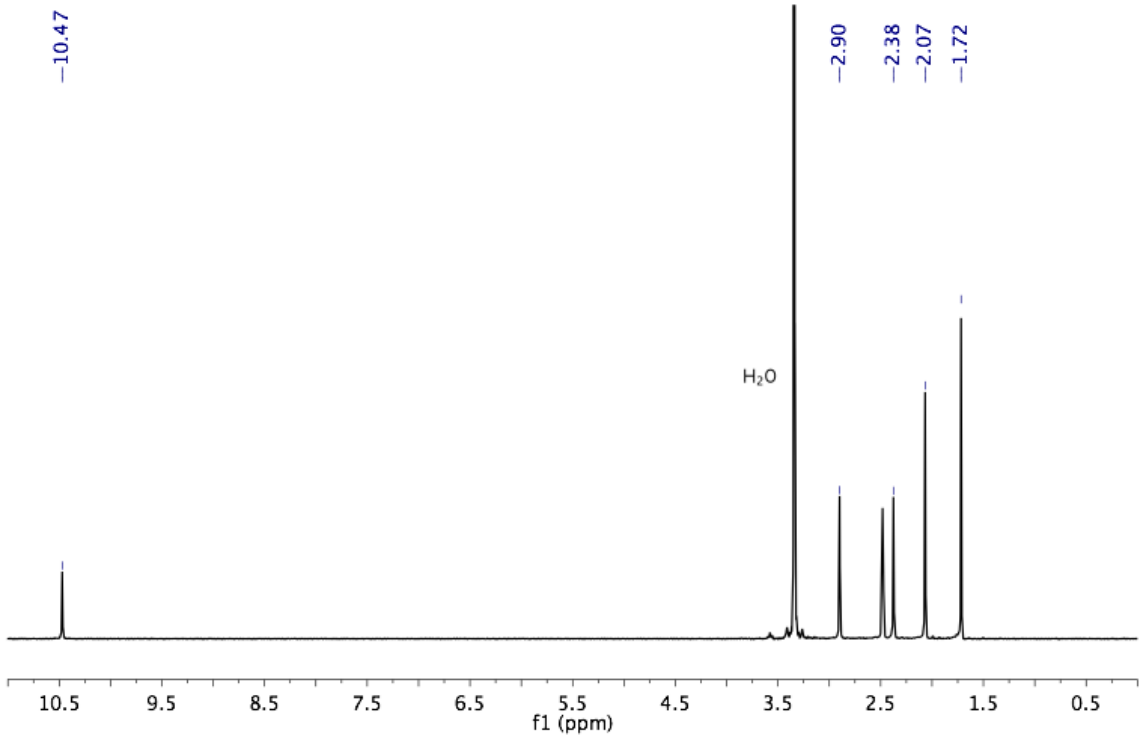

Figure S1. ^{1}H NMR spectrum of **HON_4OH** in DMSO-d_6 at 25 ºC.

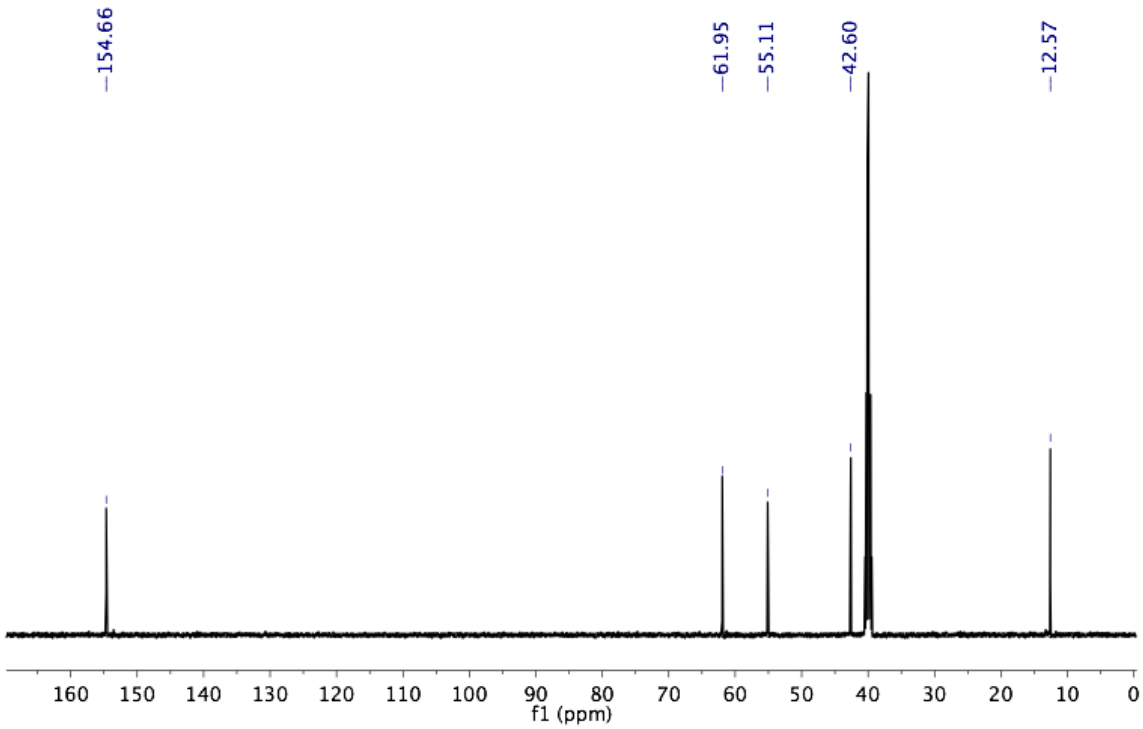

Figure S2. $^{13}C\{^{1}H\}$ NMR spectrum of **HON_4OH** in DMSO-d_6 at 25 ºC.

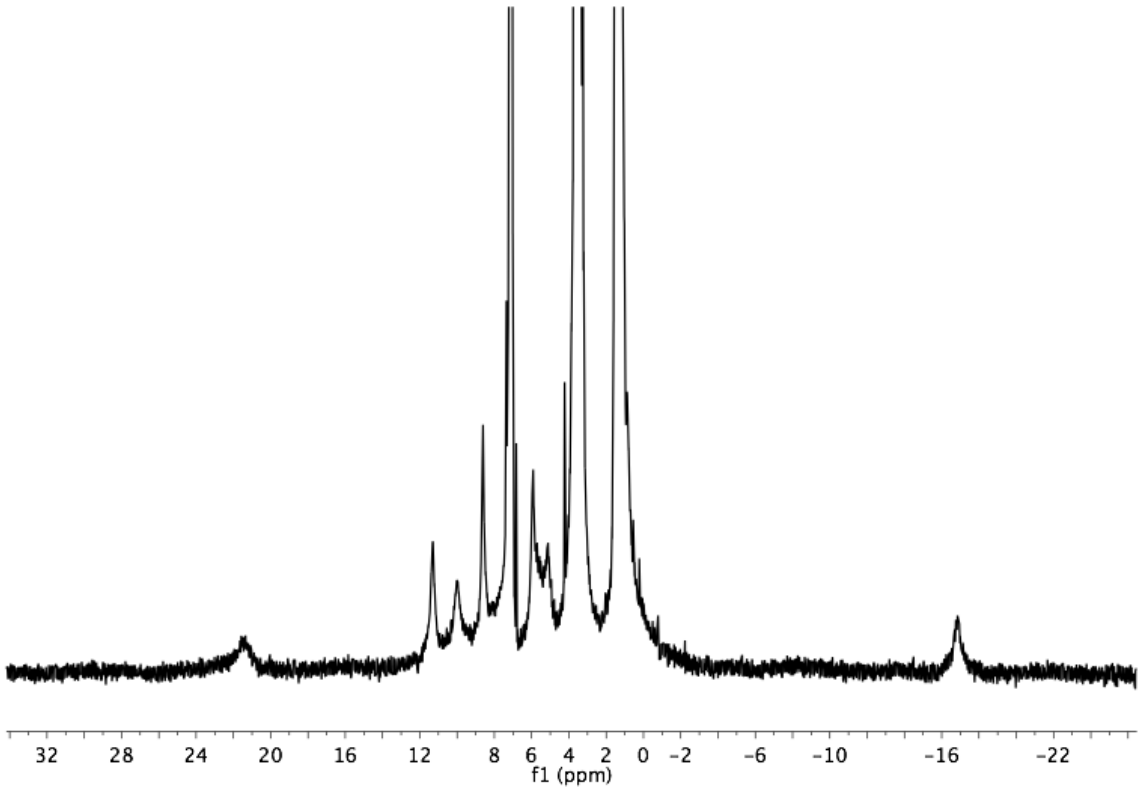

Figure S3. ^{1}H NMR spectrum of **$LMn^{IV}_3CaO_4(OAc)_3$•THF (1)** in C_6D_6 with a drop of THF for solubility at 25 ºC.

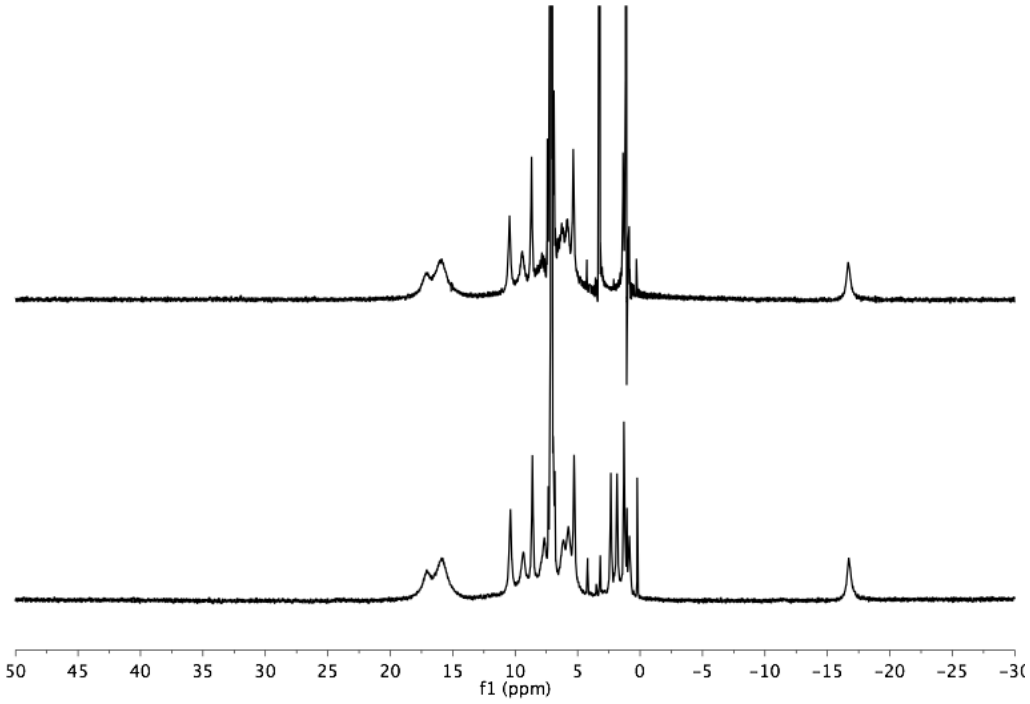

Figure S4. ^{1}H NMR spectrum of **$LMn^{III}_{2}Mn^{IV}_{2}O_{4}(OAc)_{3}$ (2)** as synthesized in the literature [3] (top), or from **1** and $Mn(OTf)_2$ (bottom). Both are in C_6D_6 at 25 ºC.

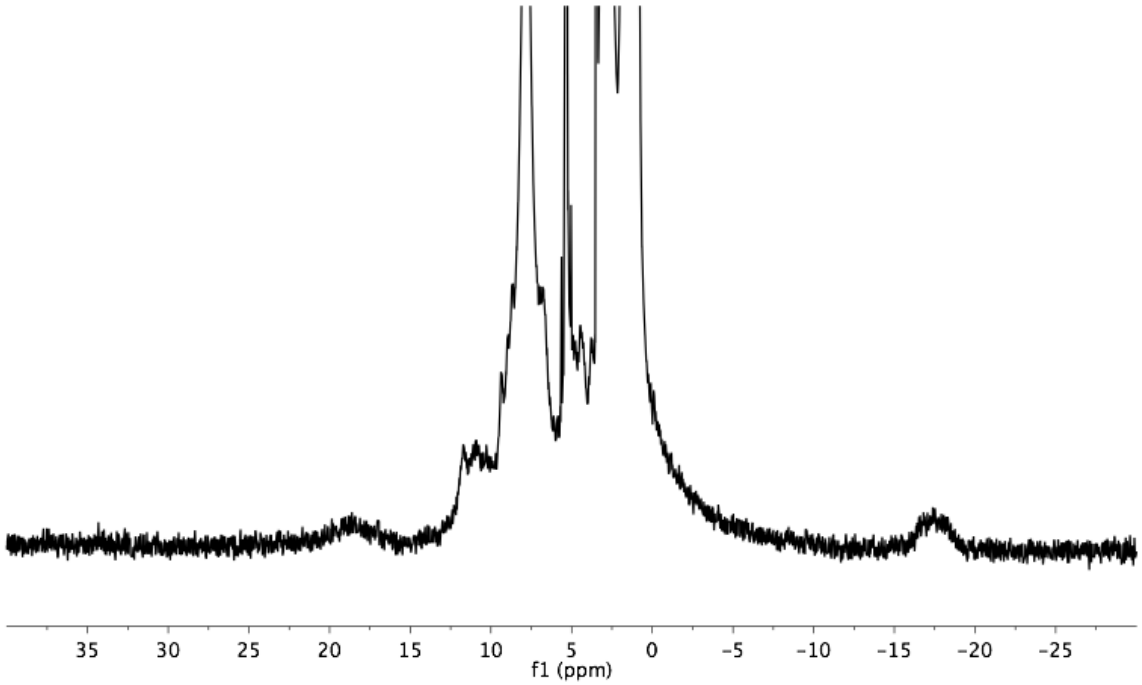

Figure S5. ^{1}H NMR spectrum of **$[LMn^{IV}_{3}GdO_{4}(ON_{4}O)(OAc)(DMF)]OTf$ (4)** in CD_2Cl_2 at 25 ºC.

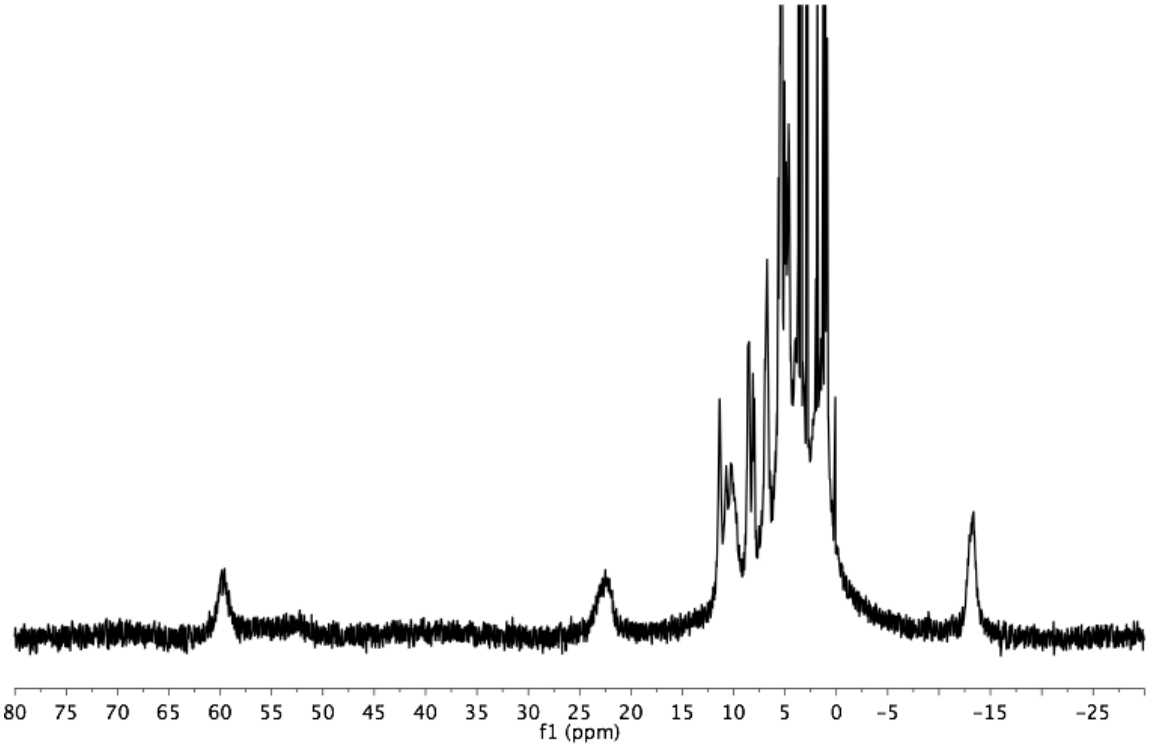

Figure S6. ^{1}H NMR spectrum of **LMn$^{IV}_{3}$CaO$_4$(ON$_4$O)(OAc) (5)** in CD_2Cl_2 at 25 ºC.

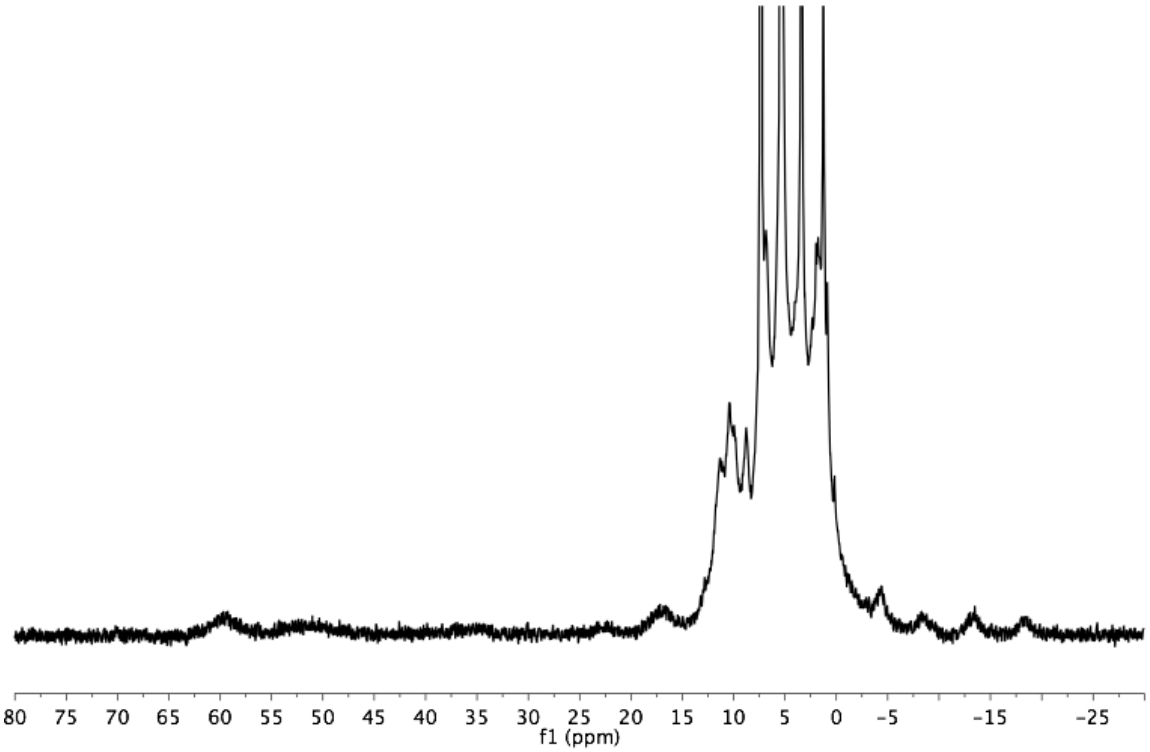

Figure S7. ^{1}H NMR spectrum of **[LMn$^{IV}_{3}$CaO$_3$(OH)(ON$_4$O)(OAc)]OTf (6)** in CD_2Cl_2 at 25 ºC.

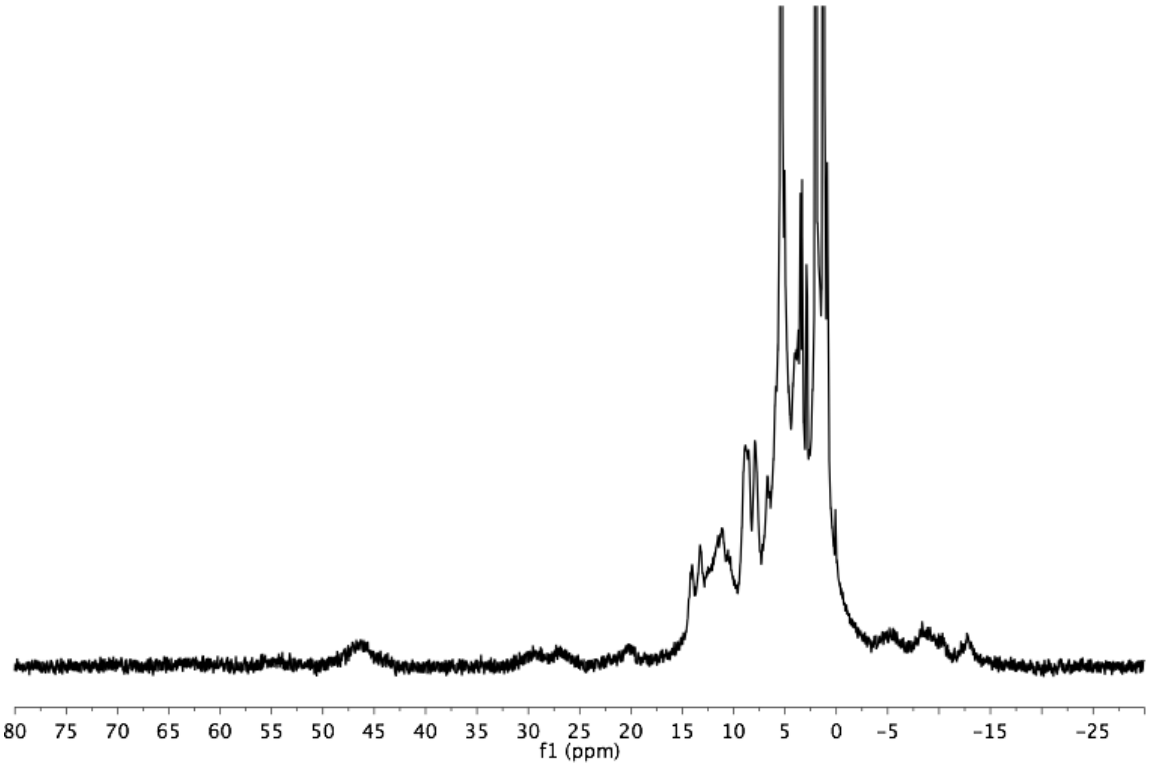

Figure S8. ^{1}H NMR spectrum of **LMn$^{IV}_{3}$CaO$_4$(ON$_4$O)(OAc)Ag(OTf) (7)** in CD_2Cl_2 at 25 ºC.

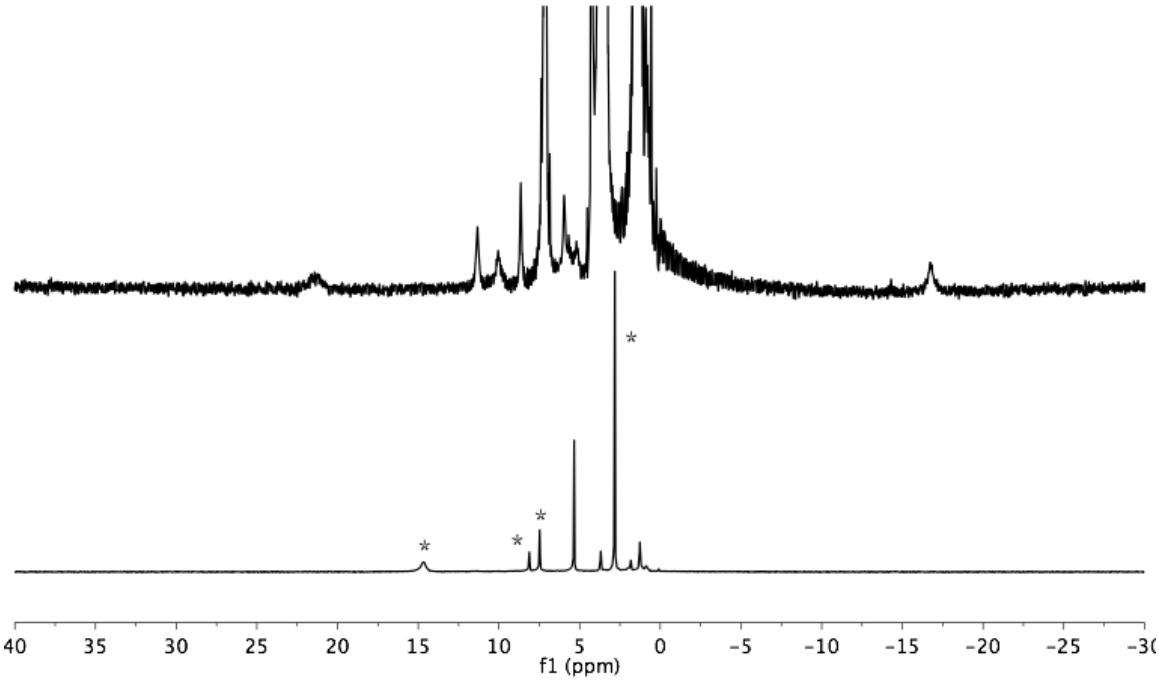

Figure S9. ^{1}H NMR spectra of the CH_2Cl_2 fraction (bottom, with peaks of LutHOTf starred, CD_2Cl_2 at 25 ºC) and benzene fraction (top, C_6D_6 w/ drop of THF, 25 ºC) of the non-reaction of 1 and LutHOTf.
The paramagnetic peaks of the top spectrum match those of pure **1** (Figure S3).

ESI Mass Spectra

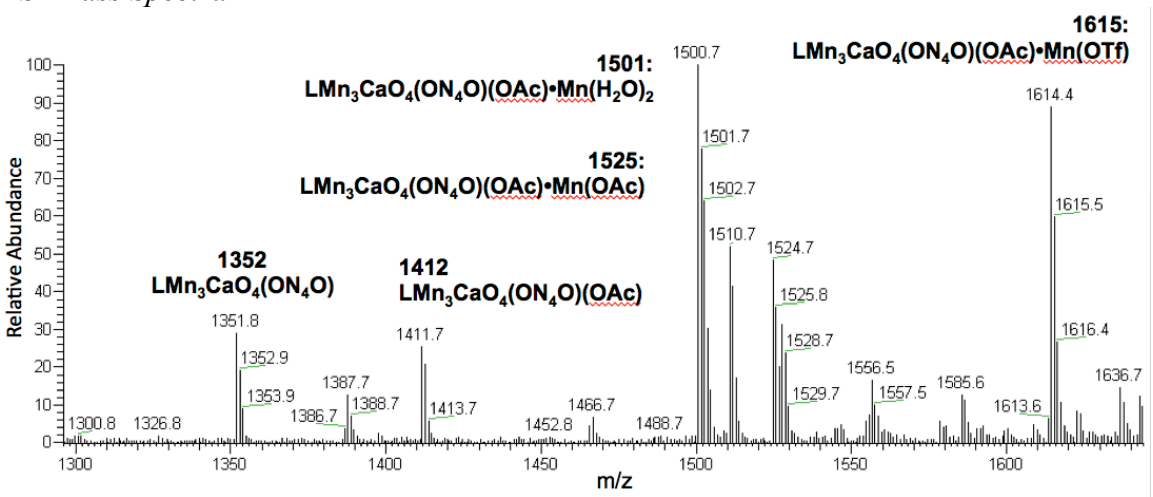

Figure S10. ESI-MS of an aliquot from the reaction of **5** with $Mn(OTf)_2$.

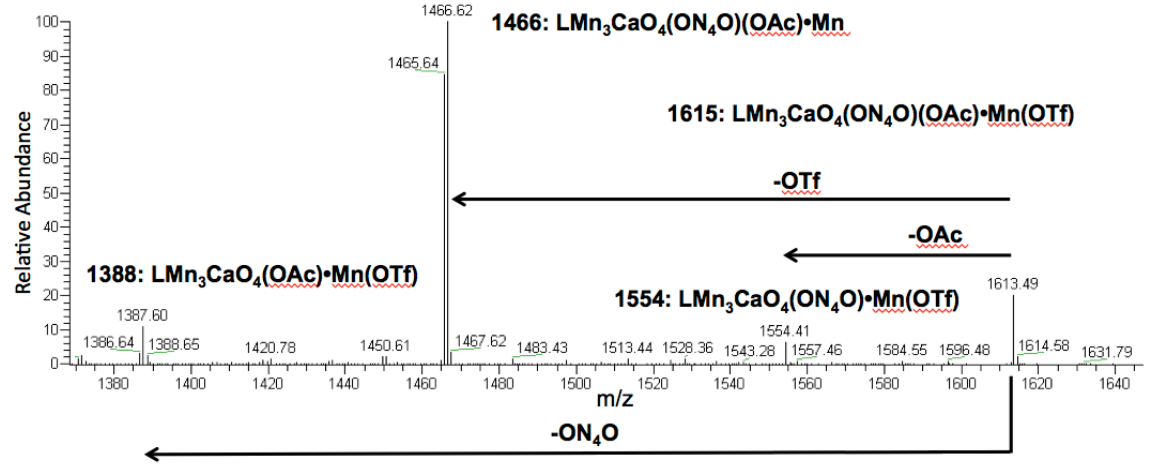

Figure S11. Fragmentation (ms/ms) mode ESI-MS on the *m/z* 1615 peak from the reaction of **5** with $Mn(OTf)_2$.

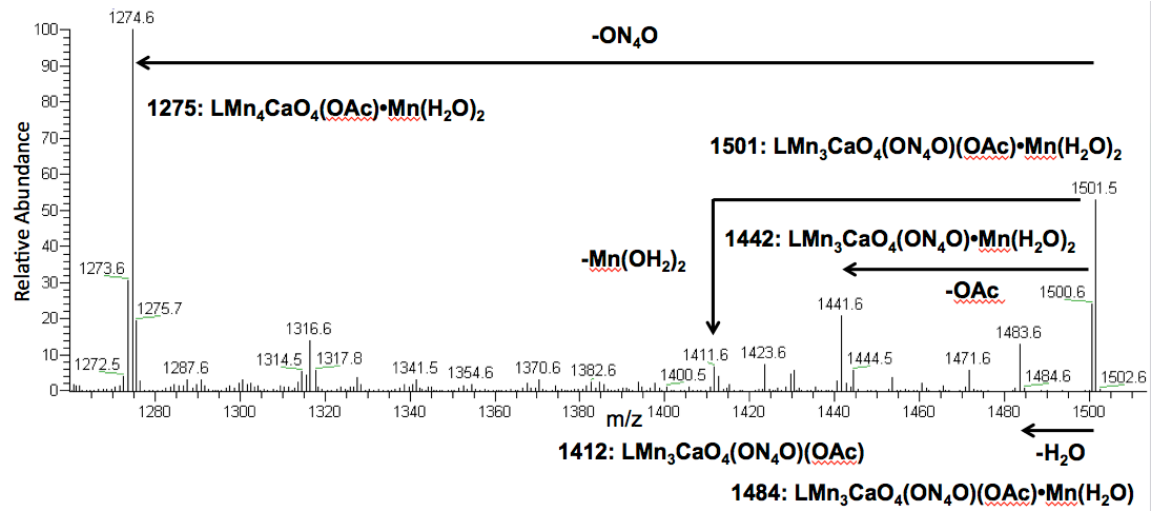

Figure S12. Fragmentation (ms/ms) mode ESI-MS on the *m/z* 1501 peak from the reaction of **5** with $Mn(OTf)_2$.

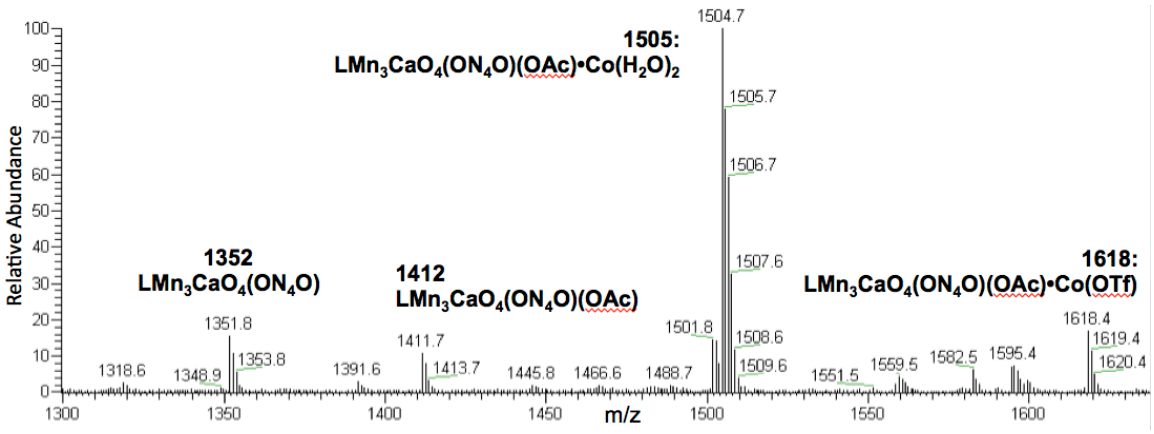

Figure S13. ESI-MS of an aliquot from the reaction of **5** with $Co(OTf)_2$.

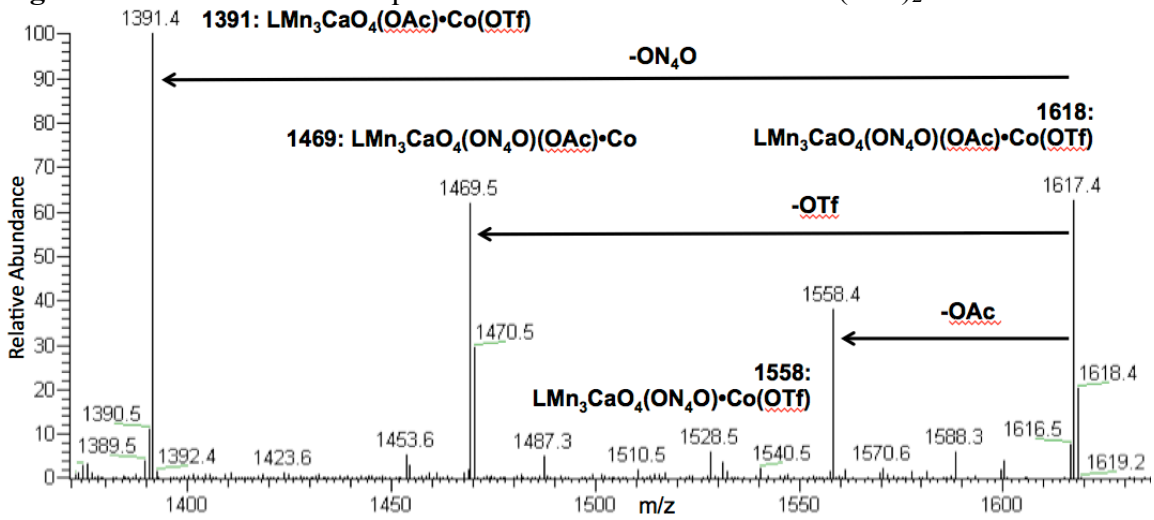

Figure S14. Fragmentation (ms/ms) mode ESI-MS on the *m/z* 1618 peak from the reaction of **5** with $Co(OTf)_2$.

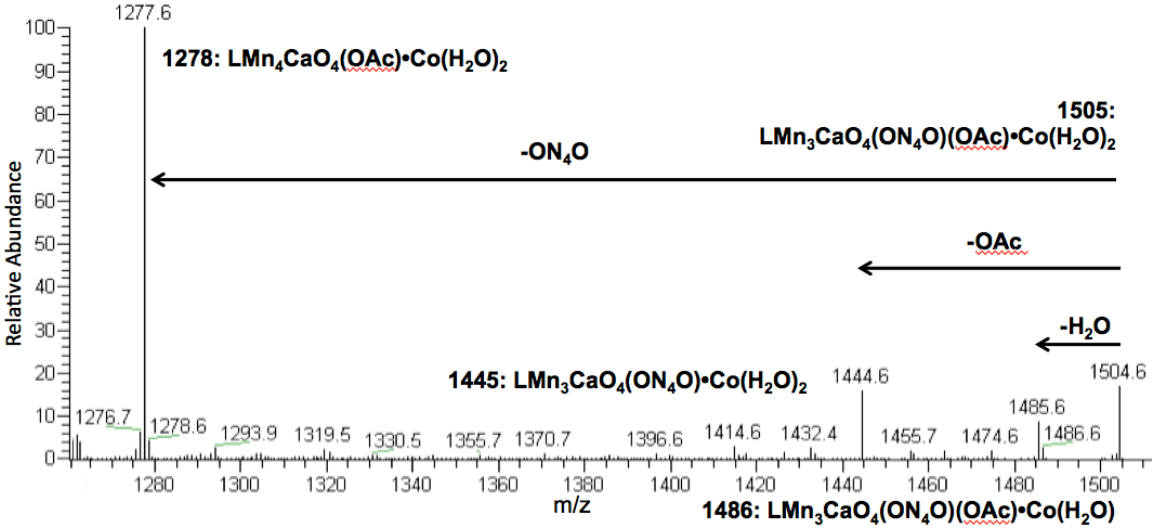

Figure S15. Fragmentation (ms/ms) mode ESI-MS on the *m/z* 1505 peak from the reaction of **5** with $Co(OTf)_2$.

Crystallographic Information

Special Refinement Details

Crystallographic data have been deposited at the Cambridge Crystallographic Database Centre, and copies can be obtained on request, free of charge, by quoting the publication citation and the deposition numbers 1018270 (**4**), 1018269 (**6**), and 1018268 (**7**)**.**

Refinement of F2 against ALL reflections. The weighted R-factor (wR) and goodness of fit (S) are based on F2, conventional R-factors (R) are based on F, with F set to zero for negative F2. The threshold expression of F2 > 2σ(F2) is used only for calculating R-factors(gt) etc. and is not relevant to the choice of reflections for refinement. R-factors based on F2 are statistically about twice as large as those based on F, and R-factors based on ALL data will be even larger.

Low-temperature diffraction data (ϕ-and ω-scans) were collected on a Bruker Kappa diffractometer coupled to an Apex II CCD detector with graphite monochromated Mo K_α radiation (λ = 0.71073 Å). The structures were solved by direct methods using SHELXS[9] and refined against F^2 on all data by full-matrix least squares with SHELXL-2014[10] using established refinement techniques.[11] Unless otherwise noted, all non-hydrogen atoms were refined anisotropically. All hydrogen atoms were included into the model at geometrically calculated positions and refined using a riding model. The isotropic displacement parameters of all hydrogen atoms were fixed to 1.2 times the *U* value of the atoms they are linked to (1.5 times for methyl groups). Unless otherwise noted, all disordered atoms were refined with the help of similarity restraints on the 1,2- and 1,3-distances and displacement parameters as well as rigid bond restraints for anisotropic displacement parameters. The high angle data for all three compounds is weak which resulted in lower resolution data collected for compounds 6 and 7.

Compound **4** crystallizes in the triclinic space group *P*-1 with one molecule in the asymmetric unit along with a triflate anion, diethyl ether and water. The triflate anion was disordered over two positions. The occupancy of the two anions refined to 0.508(8):0.495(8). The diethyl ether was also disordered over two positions. The occupancy of the two molecules refined to 0.635(11):0.365(11). The anisotropic displacement parameters for one of the diethyl ether molecules refined negative so the anisotropic displacement parameters for that molecule (O11S, C11S, C12S, C13S, C14S) were constrained to be equivalent. The hydrogen atoms for the water molecule could not be located in the difference Fourier synthesis and were not included in the model.

Compound **6** crystallizes in the triclinic space group *P*-1 with one molecule in the asymmetric unit along with a triflate anion, benzene, diethyl ether and water. Two of the benzene molecules were modeled as two component disorders. The occupancy of these disordered molecules refined to 0.31(4):0.69(4) and 0.546(3):0.454(3), respectively. A second solvent accessible void was modeled as mixture of three mutually exclusive benzene molecules, one of which is located near a crystallographic inversion center and disordered accordingly. The occupancy of the three components refined to 0.667(10):0.333(5):0.167(5). A third solvent accessible void is located near a crystallographic inversion center and modeled as a mixture of two diethyl ether and one benzene molecule. The occupancy of the three components refined to 0.201(3):0.345(3):0.454(3). The anisotropic displacement parameters for one of the

diethyl ether molecules refined negative so the anisotropic displacement parameters for that molecule (O1W, C11W, C12W, C13W, C14W) were constrained to be equivalent. All benzene solvent molecules were restrained to be flat. The highest residual electron density maxima was modeled as a water molecule. The hydrogen atoms for the water molecule could not be located in the difference Fourier synthesis and were not included in the model. The anisotropic displacement parameters for one of the carbon atoms in the acetate (C71) became negative so C71 was refined isotropically for the final refinement. The resolution of this crystal is poor with diffracted intensity to at most 0.94 Å.

Compound **7** crystallizes in the monoclinic space group *I*2/*a* with one molecule in the asymmetric unit along with 1.5 molecules of dicholoromethane and half a molecule of diethyl ether. All atoms were refined with the help of similarity restraints and enhanced rigid bond restraints for the anisotropic displacement parameters. The solvent molecules were refined with the help of similarity restraints on the 1,2- and 1,3-distances. There is an additional solvent accessible void that could not be modeled. The program SQUEEZE[12] as implemented in Platon[13] was used to remove the contribution of the disordered solvent to the structure factors.

The data for **7** is poor with diffraction data to at most 1.15 Å. In addition the diffraction reflections are smeared and the sample does not appear to be a single crystal. Although the quality of this structure is poor, it represents the best possible data obtained after multiple recrystallization attempts. Due to the poor quality of the data the identity of the silver atom is not certain, however, the chemical coordination, bond distances, and displacement parameters are consistent with silver over manganese or calcium.

Table S1. Crystal and refinement data for complexes **4**, **6**, and **7**.

	4	**6**	**7**
empirical formula	$C_{77}H_{81}F_3GdMn_3N_{11}O_{17}S$	$C_{93.91}H_{91.19}CaF_3Mn_3N_{10}O_{15.55}S$	$C_{74}H_{71}AgCaC_{3.5}F_3Mn_3N_{10}O_{14.5}$
formula wt	1843.65	1902.55	1858.31
T (K)	100(2)	100(2)	100(2)
a, Å	14.8835(10)	13.9463(15)	31.574(4)
b, Å	16.1532(11)	16.9456(18)	17.923(2)
c, Å	16.7758(11)	21.456(2)	32.134(6)
α, deg	88.985(3)	101.260(3)	90
β, deg	89.785(3)	102.405(3)	119.365(3)
γ, deg	69.483(3)	102.535(3)	90
V, Å^3	3776.7(4)	4676.2(8)	15849(4)
Z	2	2	8
cryst syst	Triclinic	Triclinic	Monoclinic
space group	P-1	P-1	I_2/A
d_{calcd}, Mg/m^3	1.621	1.351	1.558
θ range, deg	1.461 to 26.442	1.553 to 22.212	1.349 to 17.999
μ, mm^{-1}	1.470	0.549	.996
abs cor	Semi-empirical from equivalents	Semi-empirical from equivalents	Semi-empirical from equivalents
GOF	1.037	1.044	2.111
R1,[a] wR2[b] (I > 2σ(I))	0.1131, 0.1574	0.1404, 0.1878	0.2258, 0.4213

[a] $R1 = \sum||F_o| - |F_c||/\sum|F_o|$. [b] $wR2 = \{\sum[w(F_o^2 - F_c^2)^2]/\sum[w(F_o^2)^2]\}^{1/2}$.

Computational Details

The desymmetrization of the electronic structure of **1** due to the coordination of $[ON_4O]^{2-}$ was studied through the inspection of Pipek-Misek localized and delocalized (canonical) molecular orbitals. The following operations were executed using the computational package Jaguar 8.4.[14] Ground-state optimizations for **1M**, **5M**, and **6M** were accomplished via density functional theory (DFT) utilizing unrestricted B3LYP-d3[15] with the lacv3p** basis on metals and 6-31G** on organics.[16] The D3 modified B3LYP functional was employed to correct for dispersion forces.[17] Before the subsequent solvation calculation, the trinucleating ligand framework was substituted with six protons: three spatially fixed protons in lieu of the rigid pyridine rings and three additional protons to correspond to the unrestrained pyridine rings. Bond analysis was similarly preformed on **5** in which a crystal structure was not obtained. Next, the delocalized and localized orbitals were obtained in tandem using the B3LYP-d3 functional and larger basis set lacv3p**++ for metals Ca/Mn and 6-311G**++ for organics. The solvation calculation was accomplished in DMF solvent. The localized molecular orbitals were generated via the Pipek-Mezey orbital localization algorithm.[18] In particular, the sum of the orbital-dependent Mulliken charges is maximized in this approach. The HOMO and LUMO frontier orbitals were computed by visually inspection of the frontier orbital centered on the cubane core. Orbitals located on organic ligand fragments were ignored. Note that for **1M**, the coordinated solvent molecule was selected as water instead of THF.

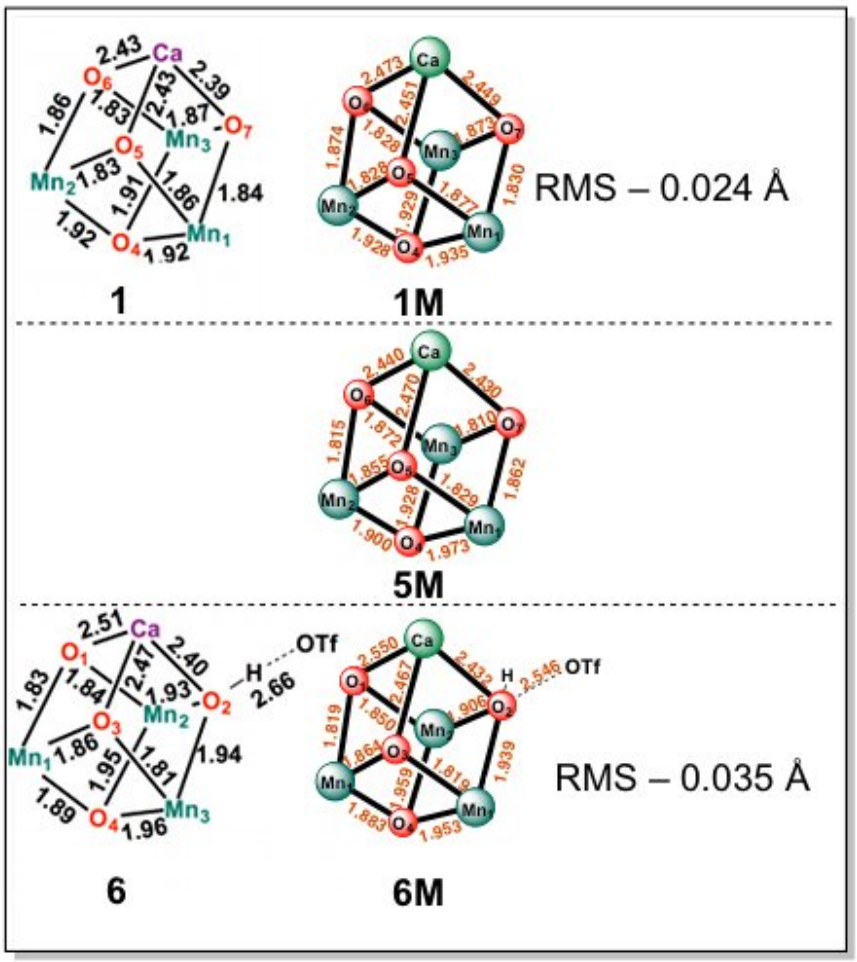

Figure S16. Bond coordinates of complexes **1**, **5**, and **6** from analysis of the DFT wavefunctions for the of truncated cubane model compared to structural parameters from the crystal structures. All reported values are measured in angstroms (Å). RMS values are calculated as 0.024 Å (1/1M) and 0.035 Å (6/6M), illustrating high geometric accuracy. Structure 5 was unable to be isolated as a crystal structure.

Table S2. Mulliken populations of complexes **1**, **5**, **6**.

1M		5M		6M	
Element	Mulliken Spin Population	Element	Mulliken Spin Population	Element	Mulliken Spin Population
Ca	0.00	Ca	0.01	Ca	0.01
Mn_1	2.93	Mn_1	2.92	Mn_1	2.87
Mn_2	2.93	Mn_2	2.92	Mn_2	2.94
Mn_3	2.93	Mn_3	2.92	Mn_3	2.86
O_4	-0.05	O_4	-0.04	O_4	0.00
O_5	0.07	O_5	0.04	O_5	0.05
O_6	0.07	O_6	0.08	O_6	0.09
O_7	0.08	O_7	0.09	O_7	0.08

The Mulliken spin population analysis for complexes **1M**, **5M**, and **6M** finds Ca^{II} and the three Mn^{IV} showing constant oxidation state during ligand exchange. No significant spin accumulates on the μ_3-oxos within the cubane core for any of the geometries.

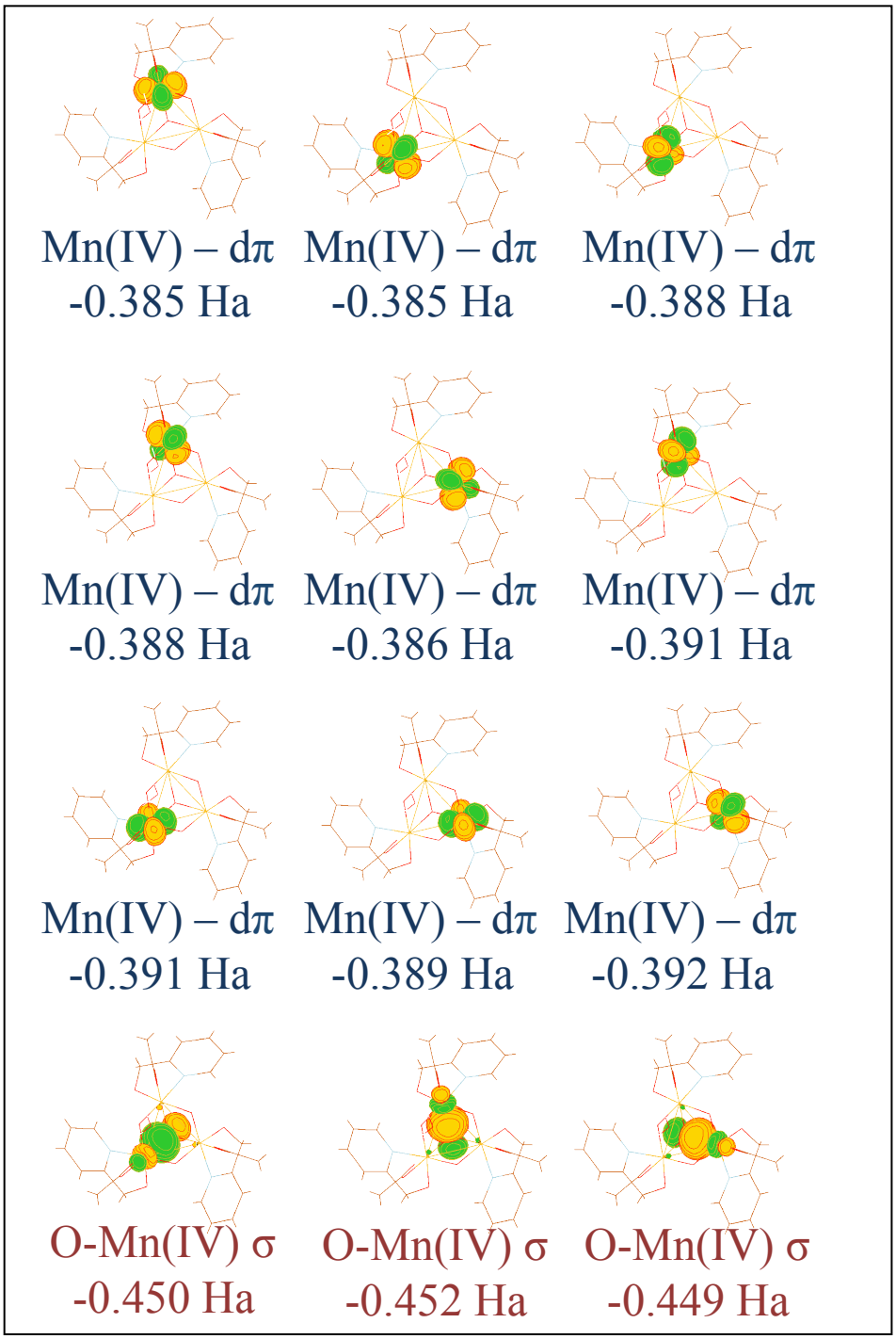

Figure S17. Pipek-Mizek Localized Orbitals and Delocalized HOMO/LUMO of **1M**.
Continued on next page.

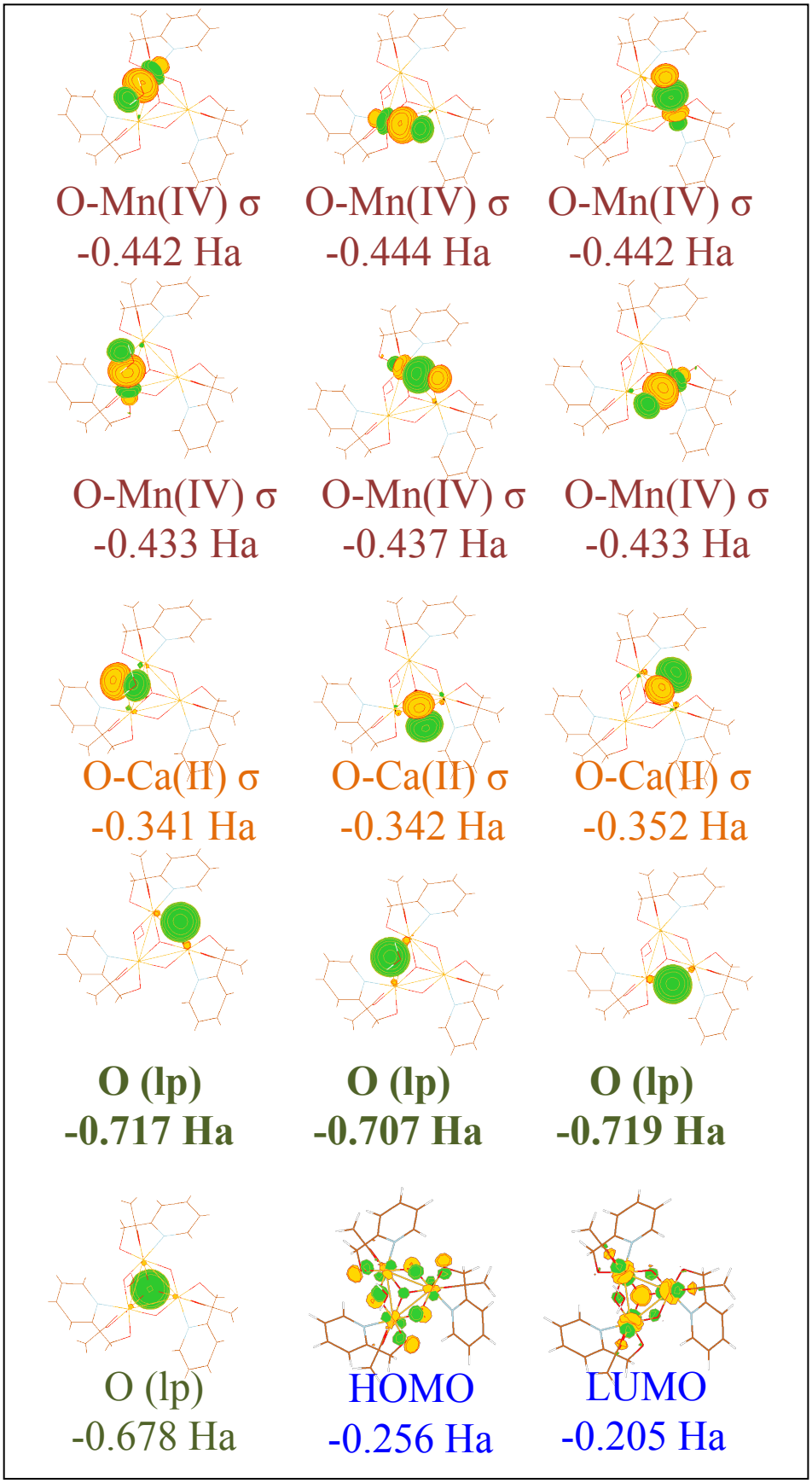
O-Mn(IV) σ
-0.442 Ha
O-Mn(IV) σ
-0.444 Ha
O-Mn(IV) σ
-0.442 Ha
O-Mn(IV) σ
-0.433 Ha
O-Mn(IV) σ
-0.437 Ha
O-Mn(IV) σ
-0.433 Ha
O-Ca(II) σ
-0.341 Ha
O-Ca(II) σ
-0.342 Ha
O-Ca(II) σ
-0.352 Ha
O (lp)
-0.717 Ha
O (lp)
-0.707 Ha
O (lp)
-0.719 Ha
O (lp)
-0.678 Ha
HOMO
-0.256 Ha
LUMO
-0.205 Ha

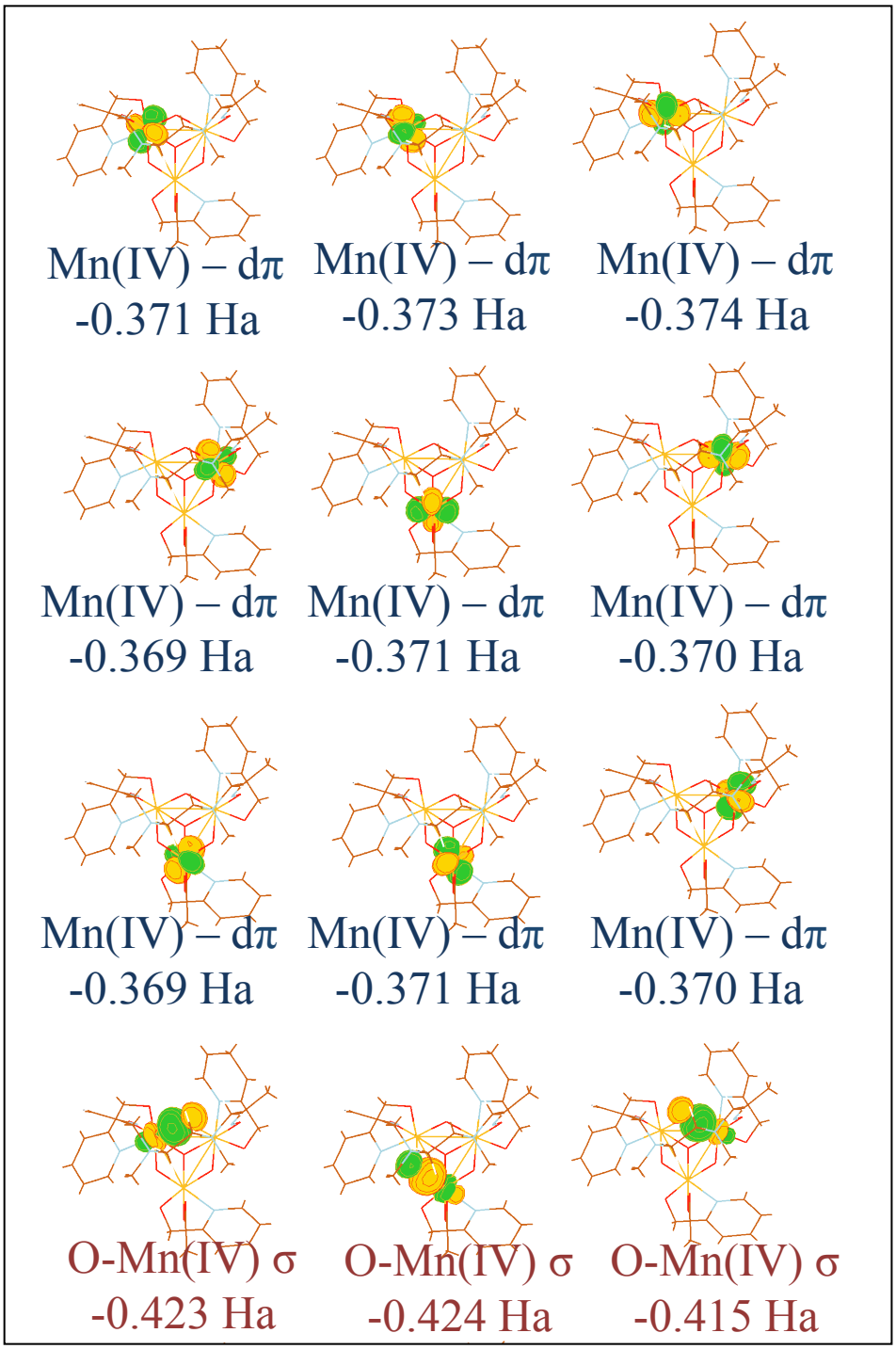

Figure S18. Pipek-Mizek Localized Orbitals and Delocalized HOMO/LUMO of **5M**.
Continued on next page.

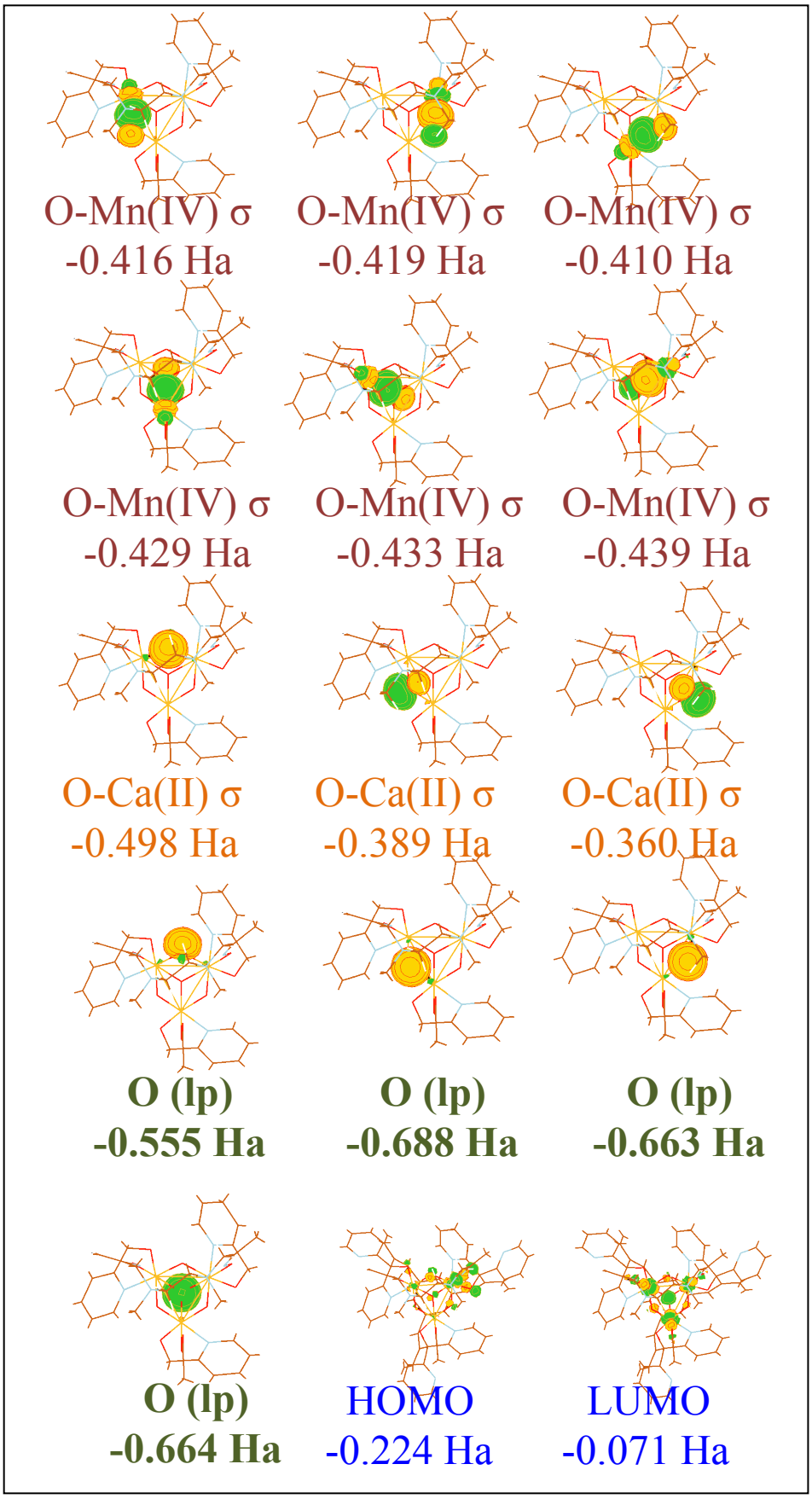
O-Mn(IV) σ
-0.416 Ha
O-Mn(IV) σ
-0.419 Ha
O-Mn(IV) σ
-0.410 Ha
O-Mn(IV) σ
-0.429 Ha
O-Mn(IV) σ
-0.433 Ha
O-Mn(IV) σ
-0.439 Ha
O-Ca(II) σ
-0.498 Ha
O-Ca(II) σ
-0.389 Ha
O-Ca(II) σ
-0.360 Ha
O (lp)
-0.555 Ha
O (lp)
-0.688 Ha
O (lp)
-0.663 Ha
O (lp)
-0.664 Ha
HOMO
-0.224 Ha
LUMO
-0.071 Ha

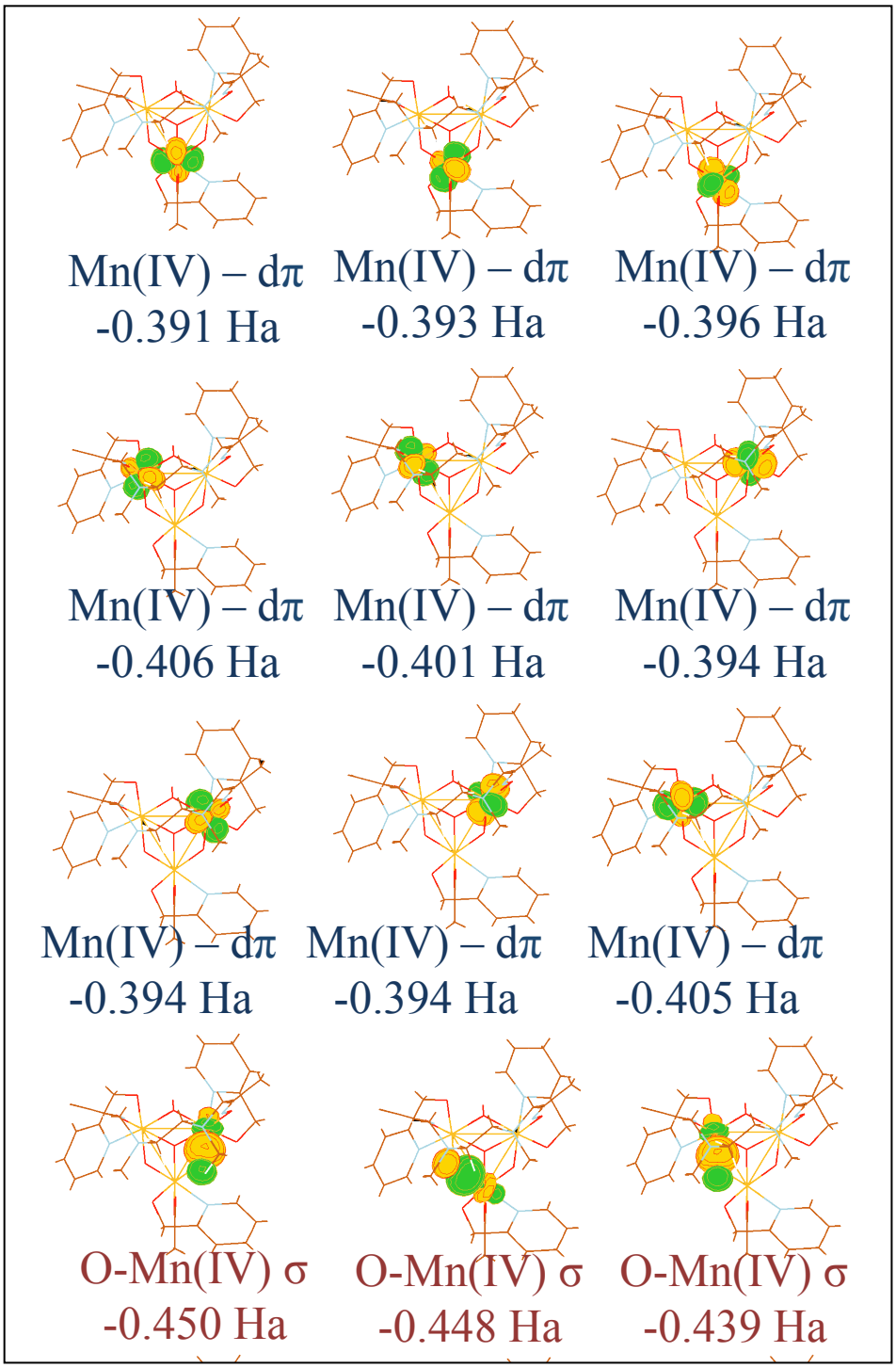

Figure S19. Pipek-Mizek Localized Orbitals and Delocalized HOMO/LUMO of **6M**. Note that the triflate ligand coordinated to the μ_3-hydroxo has been omitted for clarity. Continued on next page.

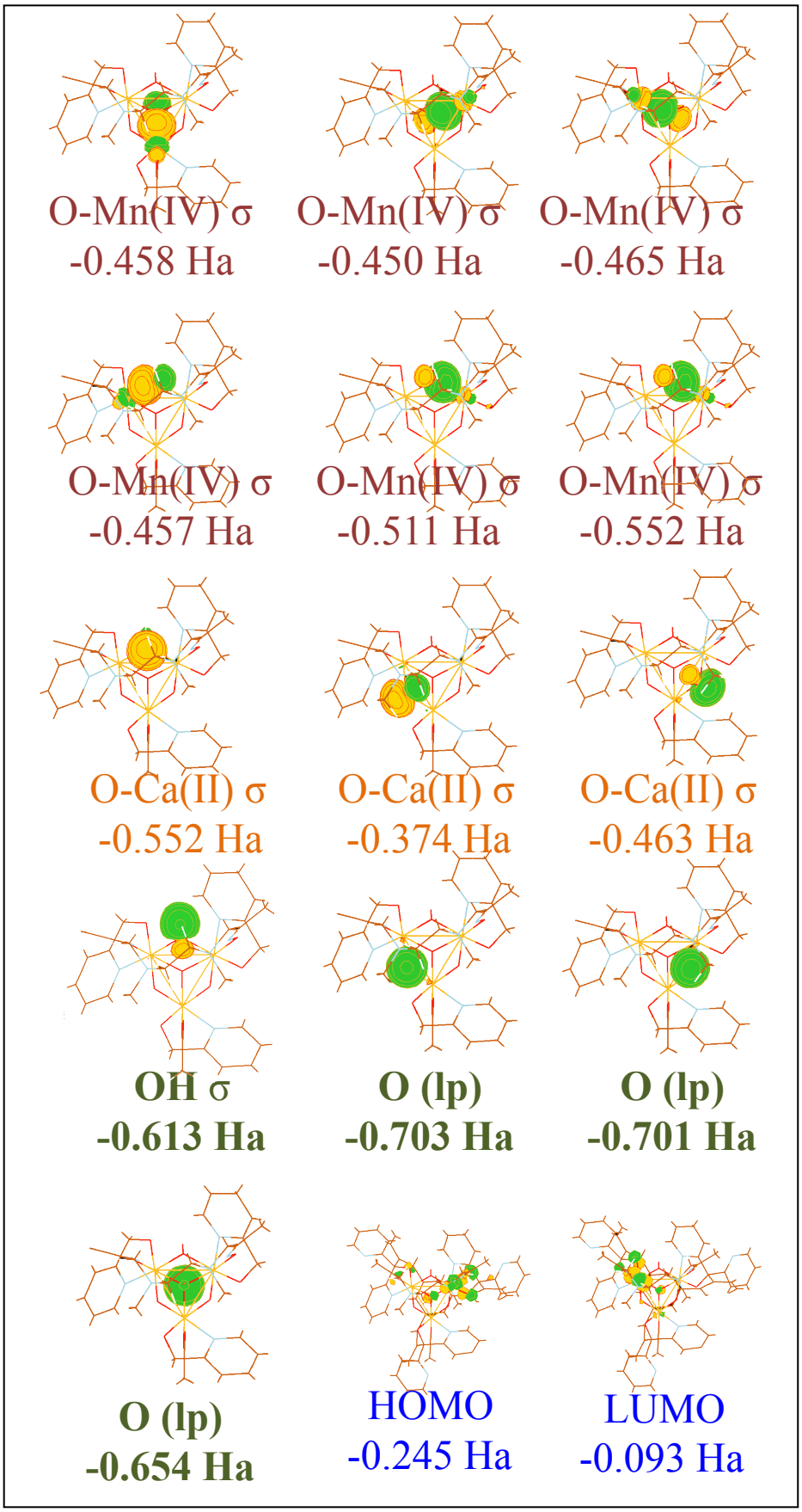
O-Mn(IV) σ
-0.458 Ha
O-Mn(IV) σ
-0.450 Ha
O-Mn(IV) σ
-0.465 Ha
O-Mn(IV) σ
-0.457 Ha
O-Mn(IV) σ
-0.511 Ha
O-Mn(IV) σ
-0.552 Ha
O-Ca(II) σ
-0.552 Ha
O-Ca(II) σ
-0.374 Ha
O-Ca(II) σ
-0.463 Ha
OH σ
-0.613 Ha
O (lp)
-0.703 Ha
O (lp)
-0.701 Ha
O (lp)
-0.654 Ha
HOMO
-0.245 Ha
LUMO
-0.093 Ha

References

1. Pangborn, A. B.; Giardello, M. A.; Grubbs, R. H.; Rosen, R. K.; Timmers, F. J. *Organometallics* **1996,** *15*, 1518-1520.
2. Dilman, A. D.; Tishkov, A. A.; Lyapkalo, I. M.; Ioffe, S. L.; Strelenko, Y. A.; Tartakovsky, V. A. *Synthesis* **1998**, 181-185.
3. Kanady, J. S.; Mendoza-Cortes, J. L.; Tsui, E. Y.; Nielsen, R. J.; Goddard III, W. A.; Agapie, T. *J. Am. Chem. Soc.* **2013,** *135*, 1073-1082.
4. Bryan, P. S.; Dabrowiak, J. C. *Inorg. Chem.* **1975,** *14*, 296-299.
5. Curley, J. J.; Bergman, R. G.; Tilley, T. D. *Dalton Trans.* **2012,** *41*, 192-200.
6. Lin, P.-H.; Takase, M. K.; Agapie, T. *Inorg. Chem.* **2014,** *Under Revision*.
7. Semakin, A. N.; Sukhorukov, A. Y.; Lesiv, A. V.; Khomutova, Y. A.; Ioffe, S. L.; Lyssenko, K. A. *Synthesis* **2007**, 2862-2866.
8. Kanady, J. S.; Tsui, E. Y.; Day, M. W.; Agapie, T. *Science* **2011,** *333*, 733-736.
9. Sheldrick, G. M. *Acta Cryst. A* **1990,** *46*, 467-473.
10. Sheldrick, G. M. *Acta Cryst. A* **2008,** *64*, 112-122.
11. Müller, P. *Cryst. Rev.* **2009,** *15*, 57-83.
12. van der Sluis, P.; Spek, A. L. *Acta Cryst. A* **1990,** *46*, 194-201.
13. Spek, A. L. *Acta Cryst. D* **2009,** *65*, 148-155.
14. Bochevarov, A. D.; Harder, E.; Hughes, T. F.; Greenwood, J. R.; Braden, D. A.; Philipp, D. M.; Rinaldo, D.; Halls, M. D.; Zhang, J.; Friesner, R. A. *Int. J. Quantum Chem.* **2013,** *113*, 2110-2142.
15. (a) Becke, A. D. *J. Chem. Phys.* **1993,** *98*, 5648-5652.(b) Lee, C. T.; Yang, W. T.; Parr, R. G. *Phys. Rev. B* **1988,** *37*, 785-789.
16. (a) Francl, M. M.; Pietro, W. J.; Hehre, W. J.; Binkley, J. S.; Gordon, M. S.; Defrees, D. J.; Pople, J. A. *J. Chem. Phys.* **1982,** *77*, 3654-3665.(b) Hehre, W. J.; Ditchfie.R; Pople, J. A. *J. Chem. Phys.* **1972,** *56*, 2257-2261.
17. Grimme, S. *J. Comput. Chem.* **2006,** *27*, 1787-1799.
18. Pipek, J.; Mezey, P. G. *J. Chem. Phys.* **1989,** *90*, 4916-4926.